Supplementary Information *for*
A Digital-Analog Memristor Based on Ru-Polymer Complex for High-Performance, Noise-Resistant AI Applications

Minghao Qi,[a] Weijia Dong,[a] Yang Han,*[a] Yunfeng Deng*[a] and Yanhou Geng[a]

a. School of Materials Science and Engineering, Tianjin Key Laboratory of Molecular Optoelectronic Science and Key Laboratory of Organic Integrated Circuits, Ministry of Education, Tianjin University, and Collaborative Innovation Center of Chemical Science and Engineering (Tianjin), Tianjin, 300072, China.

1. Supplementary figures and table

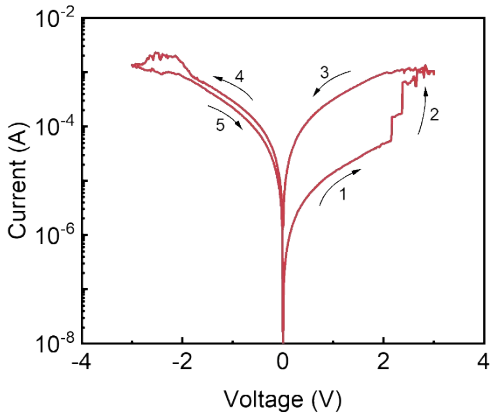

Figure S1 IV characteristic curve from the first sweep.

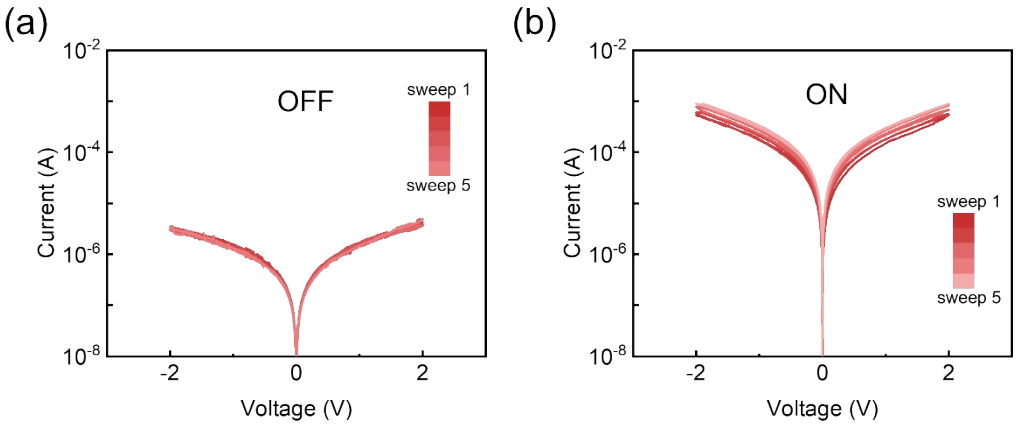

Figure S2 IV cycling curves of Ru-PVPS-based devices at 0-±2 V for the a) OFF and b)

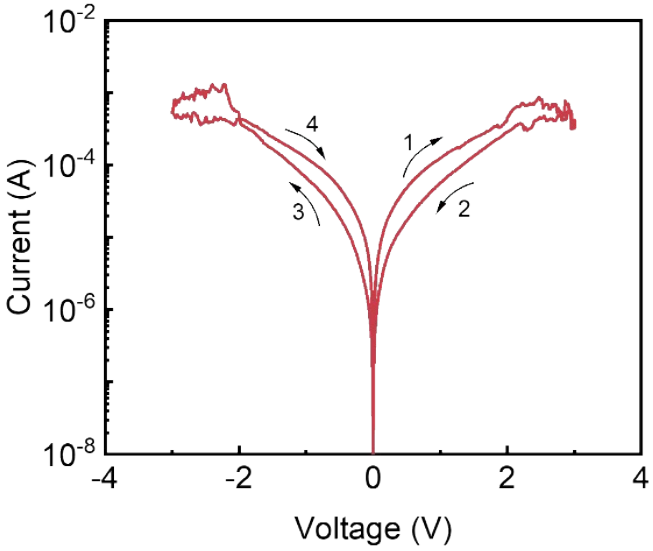

Figure S3 IV characteristic curve from the second sweep.

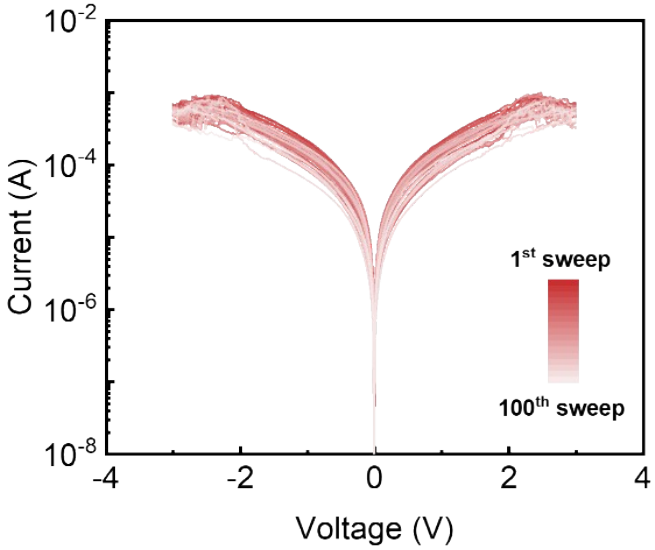

Figure S4 IV characteristic curves of 100 sweeps performed on the Ru-PVPS-based device.

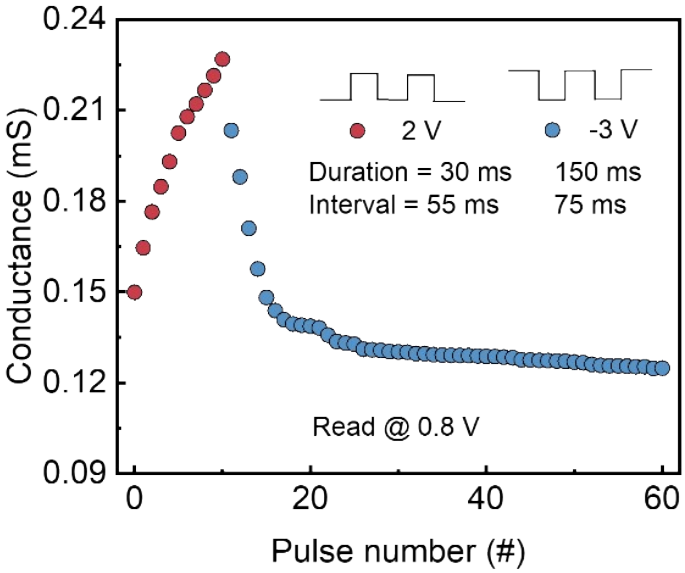

Figure S5 Induction of LTP and LTD by consecutive 2.0 V and -3.0 V pulses, respectively (10×2.0 V pulses increase conductance; 50×-3 V pulses decrease conductance).

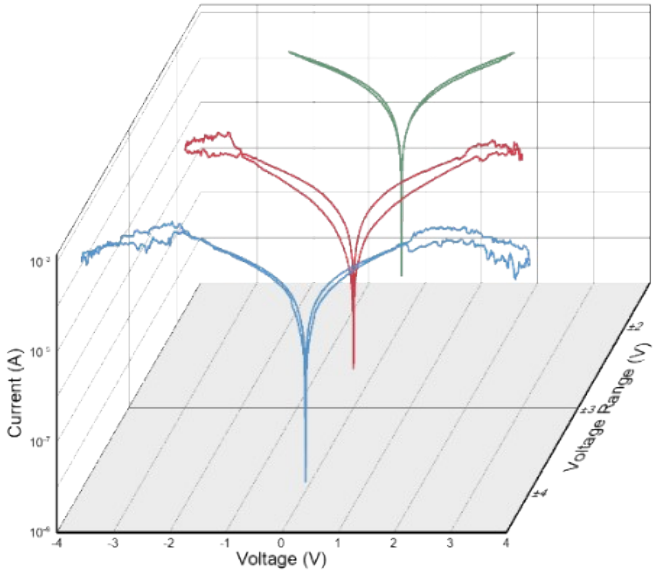

Figure S6 IV characteristic curves at different scan voltage ranges.

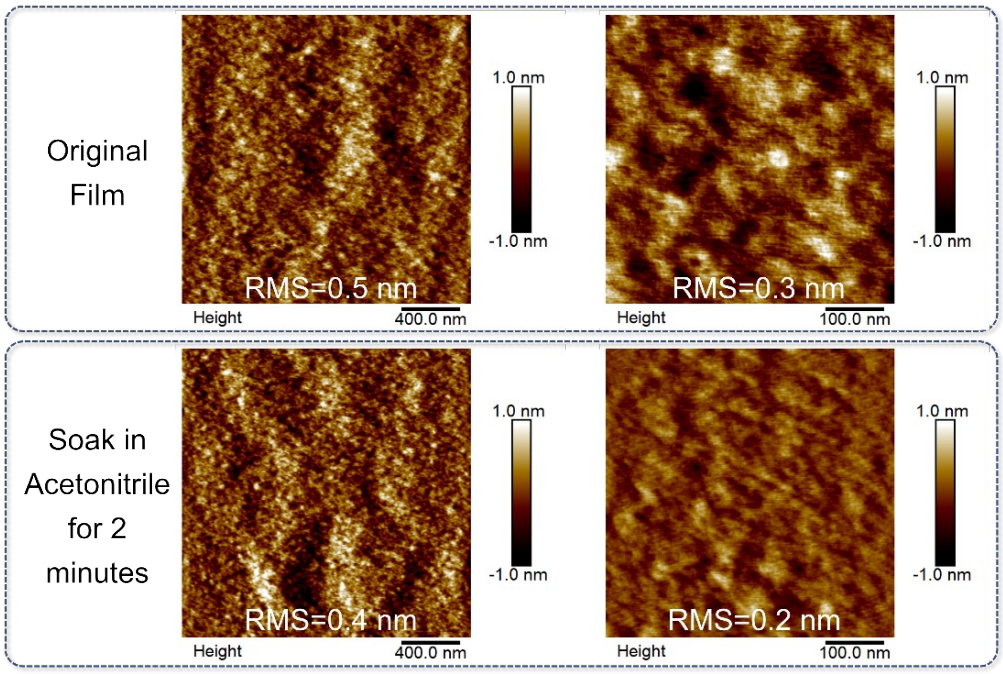

Figure S7 AFM images of Ru-PVPS film before and after acetonitrile immersion.

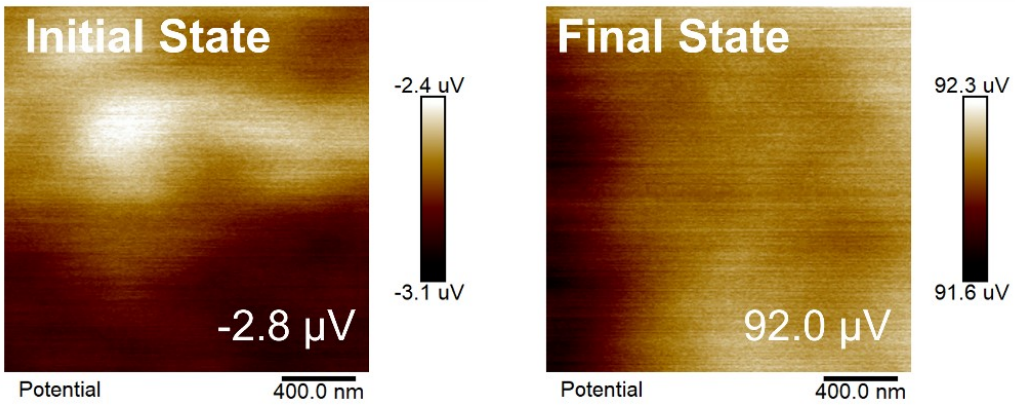

Figure S8 Surface potential of the device in the on and off states, as measured by KPFM.

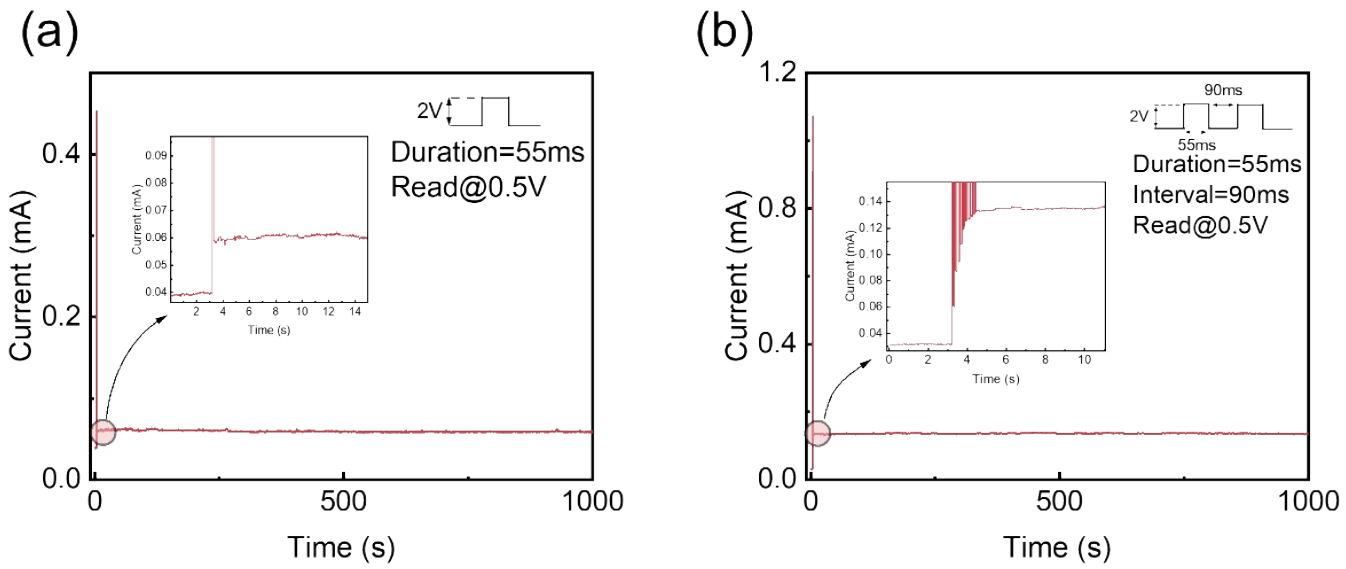

Figure S9 Retention behavior of the pulse-induced conductance states. a) 1 pulse b) 10 pulses, read at 0.5 V.

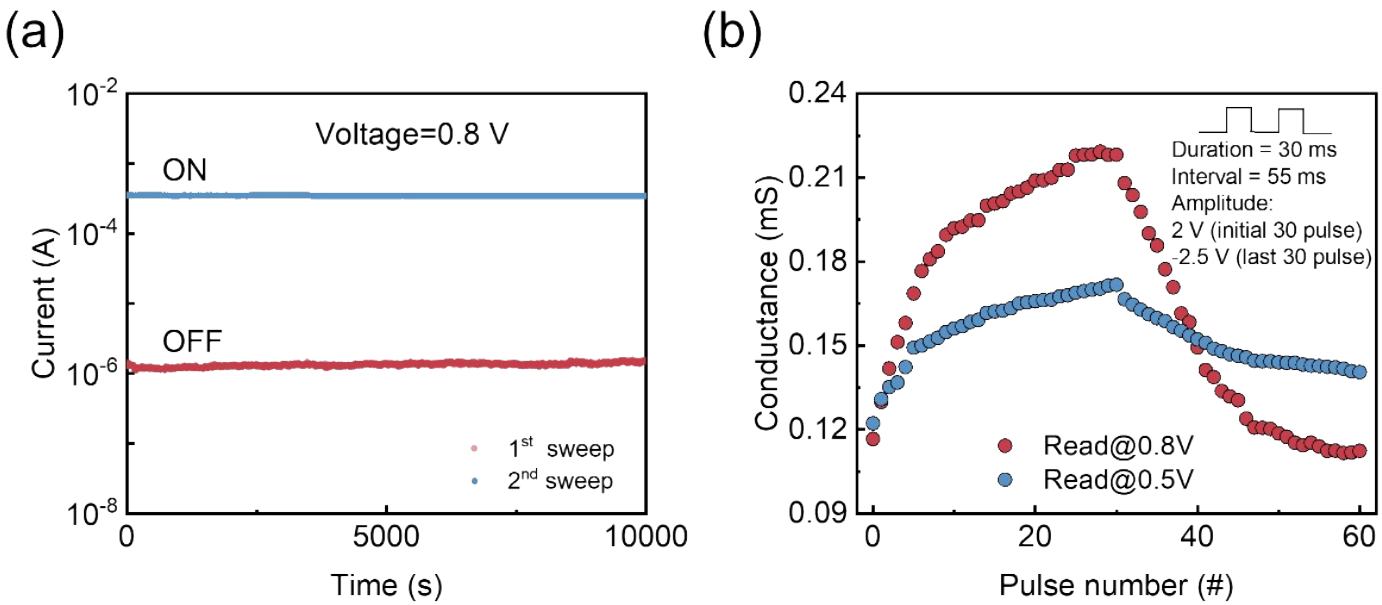

Figure S10 a) The current and retention time for the ON and OFF states read at 0.8 V. b) LTP-LTD testing by applying the same pulse voltage while varying the read voltage (0.8 V and 0.5 V).

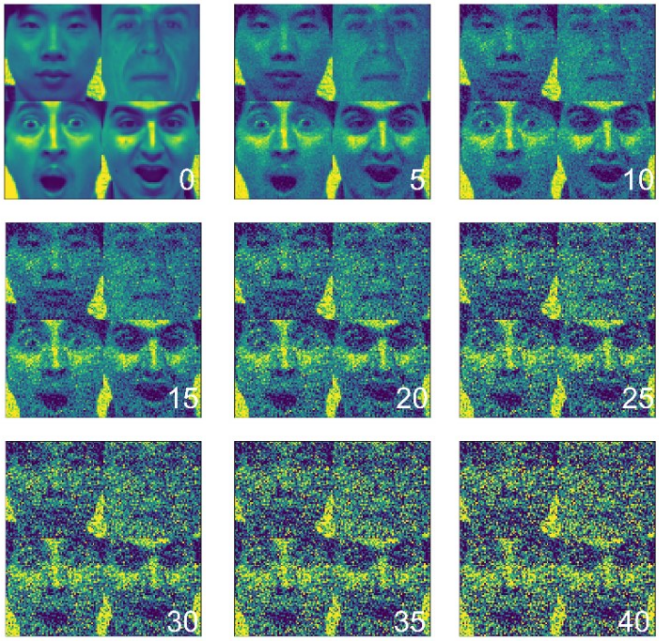

Figure S11 Facial images with varying proportions of Gaussian noise interference.

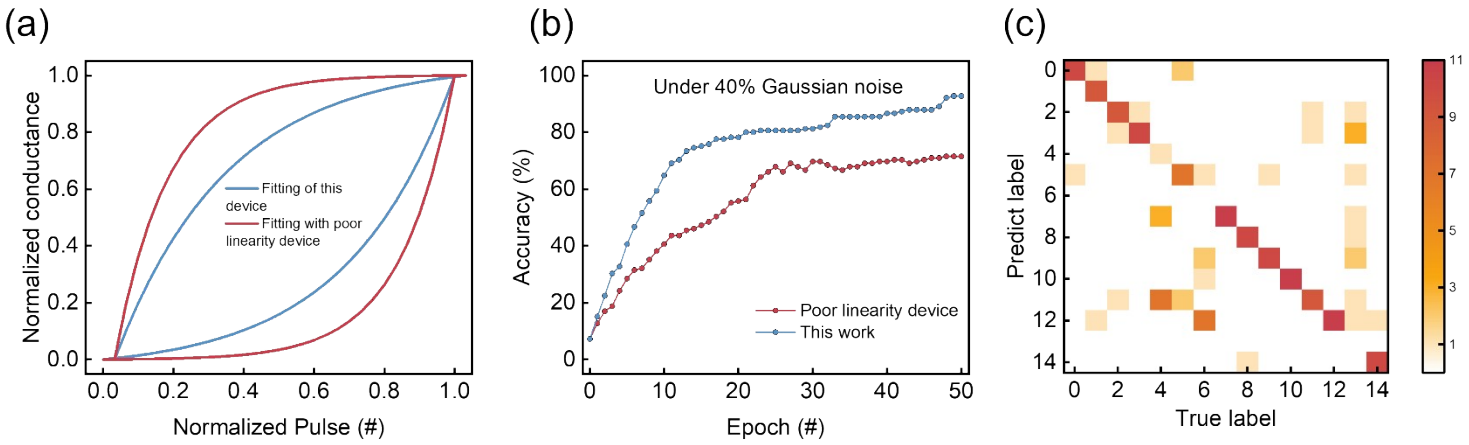

Figure S12 a) Fitting curves for LTP and LTD at different levels of linearity. b) Relationship between recognition accuracy and number of training epochs over 50 training runs.(Recognition accuracy of fitting curves with different linearities under 40% Gaussian noise) c) Confusion matrix after 50 iterations under poor linearity.

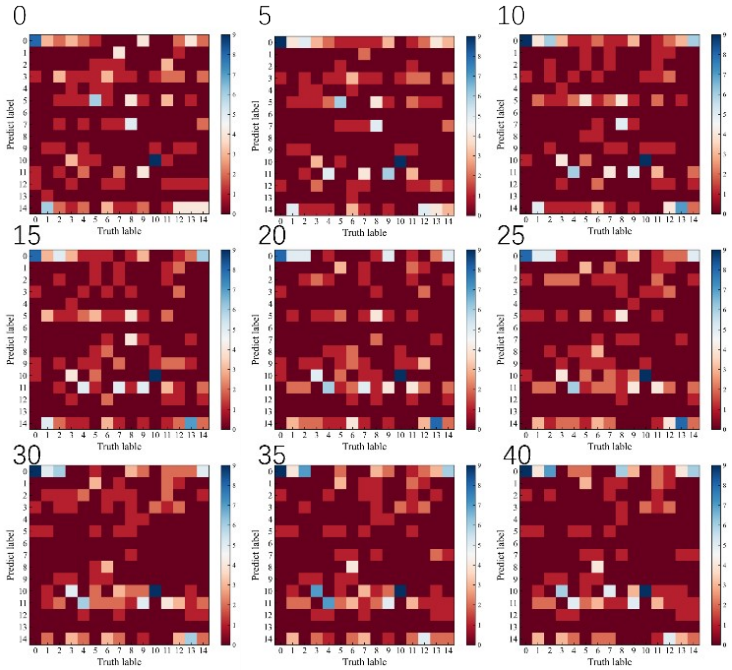

Figure S13 Confusion-matrix results for different noise levels(Before training)

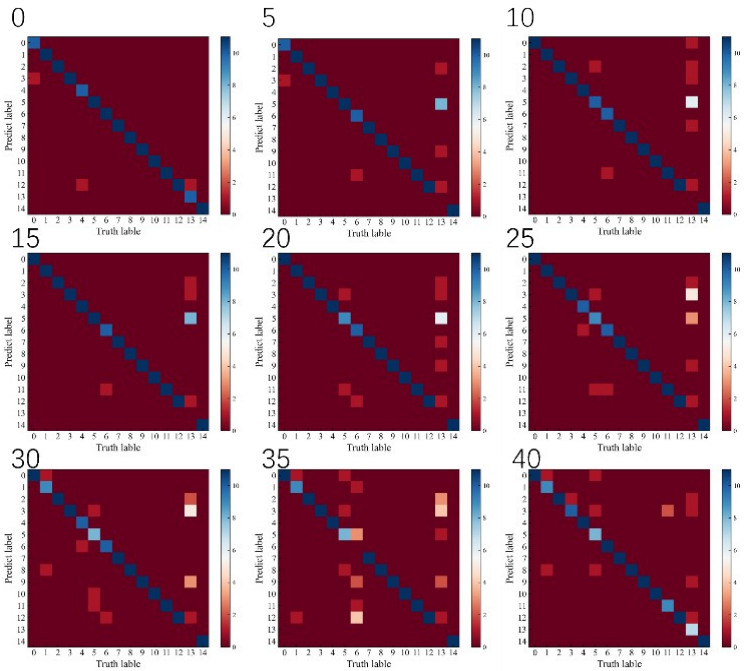

Figure S14 Confusion-matrix results for different noise levels(After training)

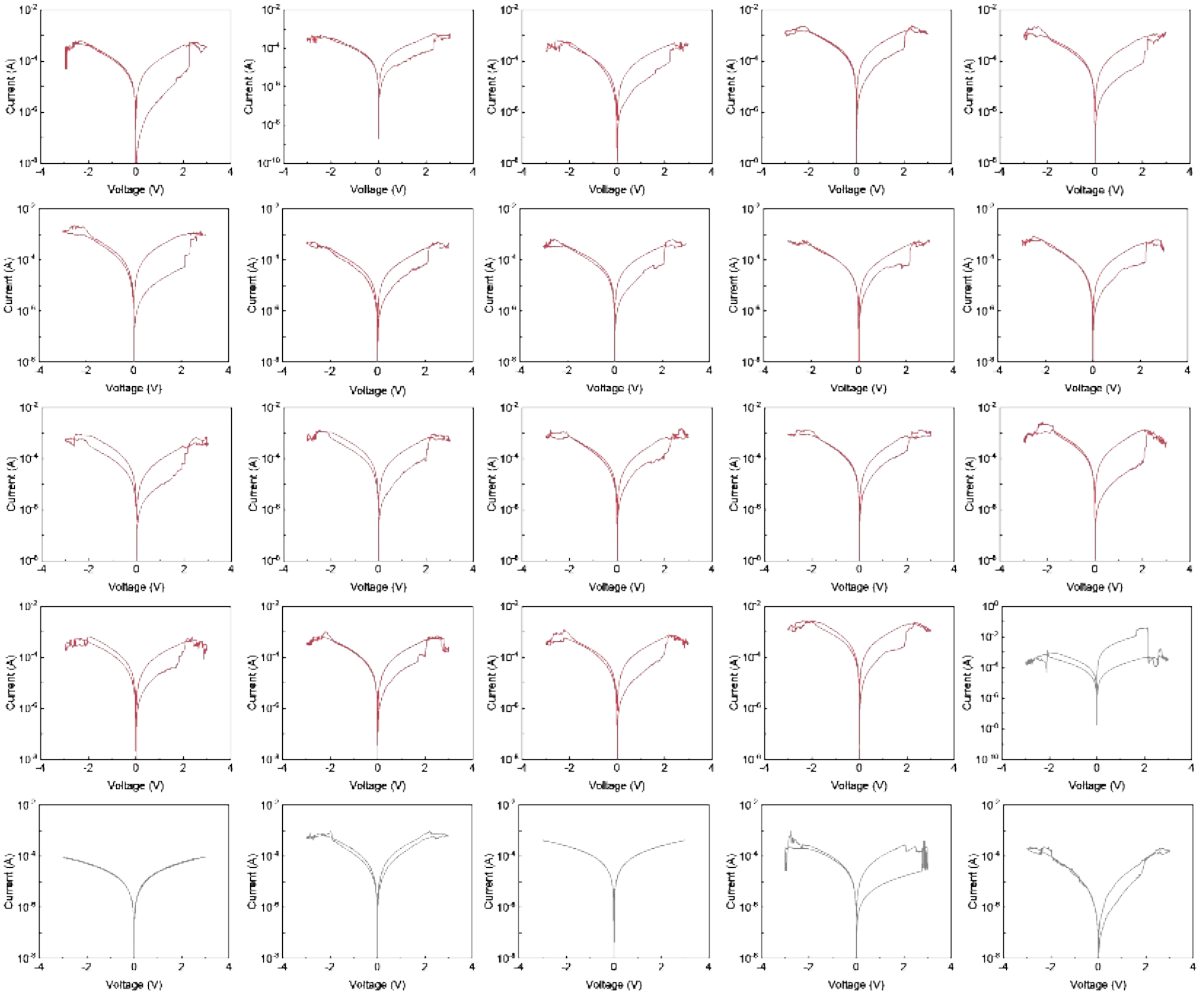

Figure S15 IV characteristics of devices within the same batch of 25 devices.

Table S1 Comparison of this work with state-of-the-art organic memristors

Device structure	On/Off ratio	Retention time (s)	Operating voltage (V)	Cycles	Applications	Ref.
Ag/PMMA/SLE/Ti	<10	10^2	1 /-1	10^2	Neuromorphic computing	[1]
Al/honey/ITO	10-10^2	10^4	3 /-3	-	Artificial synapse	[2]
Al/ 2D membrane /ITO	10^3	10^4	5 /-5	-	-	[3]
Ag/albumen:CuO/ITO/PET	10	-	6 /-6	10^2	-	[4]
Al/TMA:PVP/ITO	10^4	10^5	2 /-2	10^2	Artificial synapse	[5]
ITO/MTPP/AlO_x/Al	10	10^4	10 /-10	-	Neuromorphic computing	[6]
Au/[Ag($C_3H_4N_2$)$_2$)]NO_3/ITO	10^3	10^4	0.5 /-0.5	10^2	Logic Circuits	[7]
ITO/PEDOT:PSS/pentacene/Al	<10	-	1 /-1	-	Neuromorphic computing	[8]
Au/EDCB/Al	10^2-10^3	10^4	4 /-2	10^2	Neuromorphic computing	[9]
Au/Ru-PVPS/Au	10^2-10^3	10^4	3 /-3	10^2	Neuromorphic computing	This work

2. Experimental Section

2.1. Preparation process of the device

To ensure reliable and reproducible electrical characterization, 2×2 cm^2 Si/SiO_2 substrates (SiO_2 on the top surface, n-doped Si on the backside) are used as the support. Substrates are sequentially ultrasonically cleaned in deionized water, acetone, and isopropanol to remove particulate and organic contaminants, and then treated with ultraviolet-ozone for 30 min to further eliminate residual organics and substantially improve surface wettability, facilitating uniform spin-coating of solution films.

After cleaning, a ~30 nm Au bottom electrode was deposited by thermal evaporation. Following this, the solution was spin-coated at 1200 rpm for 90 s to form the active layer, with the spin-coating process conducted in a 70 ℃ thermal environment. (hot spin-coating).The memristor devices were then finished with the

evaporation of ~30 nm Au as the top electrodes. The chosen fabrication sequence, combining surface cleaning, electrode chemical inertness, and controlled blend composition, provided a sound platform for subsequent electrical measurements and mechanism investigations.[10]

2.2. CV Experiment

Cyclic voltammetry (CV) measurements were carried out using a CH Instruments CHI660D electrochemical workstation in a standard three-electrode configuration. A glassy carbon electrode (diameter: 6.0 mm) coated with the polymer film was used as the working electrode, a saturated calomel electrode (SCE) served as the reference electrode, and a platinum wire was used as the counter electrode.

The polymer thin films were prepared by spin-coating a solution in o-dichlorobenzene onto the surface of the glassy carbon electrode. The electrolyte solution was an anhydrous acetonitrile solution containing 0.1 mol L^{-1} tetrabutylammonium hexafluorophosphate ($TBAPF_6$). All measurements were performed at a scan rate of 0.1 V s^{-1}.

2.3. Artificial Neural Network (ANN) Simulation

The artificial neural network (ANN) simulations were performed using Python (version 3.10.15) in the PyCharm development environment. The model was constructed based on experimentally measured device characteristics to accurately reflect the real device performance.

The linearity values of long-term potentiation (LTP) and long-term depression (LTD) used in the model were 3.36 and -3.50, respectively. The relatively good linearity is considered a key factor contributing to the reliable performance of the neural network.

Matrix operations during the training process were primarily implemented using the NumPy library (version 1.26.4). Data processing, memristor array modeling,

backpropagation training, and result visualization were carried out using NumPy and Matplotlib (version 3.10.7).

2.4. IV Sweep Test

The I–V measurements were carried out using a Keysight B2900A in Quick I-V mode, with a measure delay of 0.02 s and an aperture time of 0.02 s.

3. Reference

1. K. Gao, B. Sun, B. Yang, Z. Cao, Y. Cui, M. Wang, C. Kong, G. Zhou, S. Luo, X. Chen and J. Shao, *Appl Mater Today*, 2025, **43**, 102628.
2. B. Sueoka, M. M. Hasan Tanim, L. Williams, Z. Xiao, Y. Z. Seah, K. Y. Cheong and F. Zhao, *Org Electron*, 2022, **109**, 106622.
3. Z. Zhang, Y. Nie, W. Hua, J. Xu, C. Ban, F. Xiu and J. Liu, *RSC Adv*, 2020, **10**, 20900-20904.
4. T. Guo, J. Ge, B. Sun, K. Pan, Z. Pan, L. Wei, Y. Yan, Y. N. Zhou and Y. A. Wu, *Adv Electron Mater*, 2022, **8**, 2200449.
5. A. Betal, J. Bera and S. Sahu, *J Mater Chem C*, 2023, **11**, 4674-4682.
6. Z. Wang, L. Wang, Y. Wu, L. Bian, M. Nagai, R. Jv, L. Xie, H. Ling, Q. Li, H. Bian, M. Yi, N. Shi, X. Liu and W. Huang, *Adv Mater*, 2021, **33**, 2104370.
7. C. Du, Z. Qu, Y. Ren, Y. Zhai, J. Chen, L. Gao, Y. Zhou and S.-T. Han, *Adv Funct Mater*, 2022, **32**, 2108598.
8. X. Luo, J. Ming, J. Gao, J. Zhuang, J. Fu, Z. Ren, H. Ling and L. Xie, *Front Neurosci*, 2022, **Volume 16 - 2022**.
9. W. Dong, X. Ji, C. An, C. Xu, X. Zhang, B. Zhao, Y. Liu, S. Wang, X. Yu, X. Liu, Y. Han and Y. Geng, *InfoMat*, 2025, **7**, e12659.
10. S. Goswami, R. Pramanick, A. Patra, S. P. Rath, M. Foltin, A. Ariando, D. Thompson, T. Venkatesan, S. Goswami and R. S. Williams, *Nature*, 2021, **597**, 51-56.